Nuclear Materials and Energy 12 (2017) 627–632

Contents lists available at ScienceDirect

Nuclear Materials and Energy

journal homepage: www.elsevier.com/locate/nme

Spatial distribution of atomic and ion hydrogen flux and its effect on hydrogen recycling in long duration confined and non-confined plasmas

A. Kuzmin [a,*], H. Zushi [a], I. Takagi [b], S.K. Sharma [c], M. Kobayashi [d], Y. Hirooka [d], T. Onchi [a], K. Hanada [a], N. Yoshida [a], K. Nakamura [a], A. Fujisawa [a], H. Idei [a], Y. Nagashima [a], M. Hasegawa [a], T. Mutoh [d], K. Mishra [a], H. Ohwada [e]

[a] RIAM, Kyushu University, 6-1 Kasugakoen, Kasuga, Fukuoka, 816-8580, Japan
[b] Department of Nuclear Engineering, Kyoto University, Kyoto, 615-8540, Japan
[c] Institute for Plasma Research, Ahmadabad, India
[d] National Institute for Fusion Science, 322-6 Oroshi, Toki, Gifu 509-5292, Japan
[e] IGSES, Kyushu University, 6-1 Kasugakoen, Kasuga, Fukuoka, 816-8580, Japan

ARTICLE INFO

Article history:
Received 15 July 2016
Revised 28 February 2017
Accepted 16 March 2017
Available online 27 March 2017

ABSTRACT

In order to understand the atomic hydrogen distribution in different kinds of plasma and its influence on the recycling, two kinds of plasmas were used: non-confined annular electron cyclotron resonance (ECR) and confined long duration plasmas. The permeation probes are used to measure directly the atomic hydrogen flux at several poloidal positions. The permeation through metals due to the ion and atom component of the hydrogen flux to the wall is indistinguishable. To estimate the contribution of the ions directly, Langmuir probes were used. The Γ_{inc} profile behind the plasma facing components (PFCs) is almost constant, $\sim 2 \times 10^{18}$ H/s/m^2.

1. Introduction

The retention and recycling of the hydrogen isotopes in the first wall materials of the fusion devices is an unresolved and important problem. Several approaches have been used to study hydrogen retention in-situ in the fusion devices and in the laboratory facilities. From the laboratory studies [1,2] it has been reported that the irradiation of the materials by the low-energy hydrogen atoms and ions leads to a significant hydrogen retention. Detection of the low-energy hydrogen atomic fluxes in tokamaks is a difficult task. Membrane probes could be used to resolve this problem. Several attempts with the membrane probes have been done in different tokamaks in the past twenty years [3–7]. The measurement of the neutral flux far from the walls has been done in TEXTOR and the raw signals of the permeation probes have been compared with the plasma core density and gas fuelling [3–4]. In QUEST a work was done for the past few years to develop the membrane probe system able to measure incident hydrogen flux in-situ in real time. Different types of the membranes (Ni, F82H, PdCu) were tested [5–7] and finally, the PdCu membrane was selected for the probe system. PdCu has faster response time, wider permeation regime, and higher sensitivity independent of the incident hydrogen flux. An array of the five membrane probes has been installed inside the QUEST vessel.

The poloidal distribution of the incident flux consisting of both protons and atomic hydrogen can be measured directly with the permeation probe (PP). This results are compared with the direct ion flux, measured with a Langmuir probe array (LPA) or the neutral hydrogen flux, estimated by a hydrogen Balmer line intensity (H_α). By solving a problem of the diffusion of the hydrogen atoms in metal, the permeated flux is converted to the incident flux (Γ_{inc}), and the total fluence (Φ; time integrated flux during the discharge period) is compared with the amount of the retained hydrogen. The latter is derived by global gas balance based on a difference between the external pumping and fueling amounts. This technique has been commonly carried out in the graphite and metal devices [8–10] and the amount of the retained hydrogen is determined as the difference between the injected and

* Corresponding author.
E-mail addresses: arseniy.a.kuzmin@gmail.com, kuzmin@triam.kyushu-u.ac.jp (A. Kuzmin).

http://dx.doi.org/10.1016/j.nme.2017.03.027

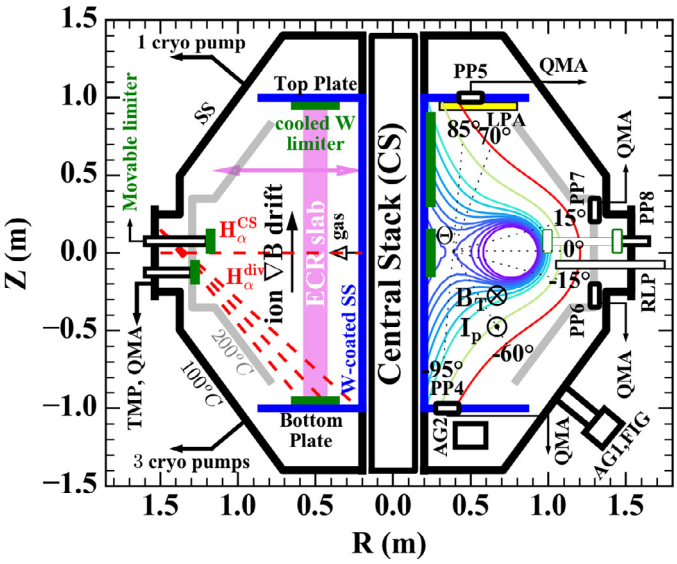

Fig. 1. QUEST vertical section schematic view. The angles, indicated in the right site correspond to poloidal position of the PPs and borders of the H_α and LP. The poloidal flux surfaces are shown for SSTO1,2. In the left side red dashed lines indicate line of sight of the hydrogen light spectroscopy. A wide magenta line (ECR slab) indicates the annular ECR plasma resonance position for ECR1-3.

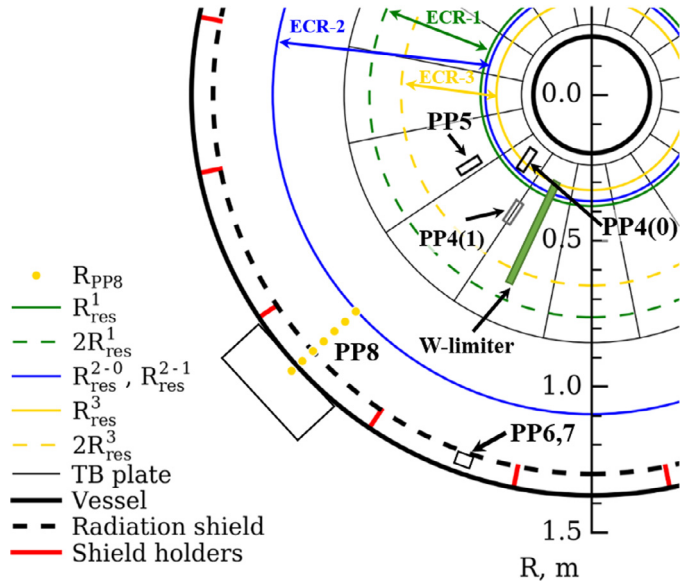

Fig. 2. QUEST horizontal section schematic view. Positions of PPs are shown. PP4(0) – position of PP4 in SSTO-2, PP4(1) – in all other cases. R_{res} – resonance positions in ECR 1-3. Rpp8 – positions of PP8 in Fig.3.

pumped out amounts of hydrogen atoms. In the case of the all-metal plasma-facing components the release of the hydrogen occurs mostly in the form of the H_2 and H_2O molecules. The former is a second order surface reaction with the recombination process. The later relates to another nonlinear processes between hydrogen and oxygen containing molecules on the surface [11]. It is also expected that atomic hydrogen irradiation of the walls will lead to the changes in the metal oxides due to formation or dissociation of the water molecules on the surfaces. In [11] it was clearly shown that efficiency of the water formation induced by the atomic hydrogen irradiation is comparable with water formation during plasma irradiation. Oxygen presence in the working gas can lead to both increase or decrease of hydrogen retention in stainless steel depending on its concentration in gas and hence on the surface. It is desirable to understand influence of the oxygen concentration in the discharges on the hydrogen retention in differently conditioned PFCs. For this purpose, water partial pressure and OII emission was analyzed in different kinds of plasma.

In the present work after a brief description of the experimental set-up in the Section 2, the poloidal distribution of the irradiation fluxes is shown in the Section 3.1, radial distribution and a role of the atomic hydrogen is shown in the Section 3.2 and gas balance results are shown in the Section 3.3. The temporal behavior of the global gas balance is discussed in the Section 4, and finally conclusion is given in the Section 5.

2. Experimental set-up

Experiments were performed in the spherical tokamak QUEST [12,13]. Details of the set-up were previously described in [7,14]. The cross sectional view of the QUEST vessel is shown schematically in Fig. 1. Two kinds of plasmas are examined in this paper: a steady electron-cyclotron resonance (ECR) slab annular plasma [15] and a steady state high poloidal beta plasma in an inboard poloidal field null (IPN) configuration [16,17]. The slab plasmas are produced by electron-cyclotron waves (ECW) at 2.45 GHz ($<$ 10 kW) or 8.2 GHz ($\sim$ 20 kW) without the poloidal field. A vertically elongated slab plasma is formed near the cyclotron resonance position and diffuses towards the side wall. The plasma-wall interaction (PWI) regions are mainly restricted on the top/bottom (TB) plates. IPN plasma has been achieved by 8.2 GHz (60 kW) with the highly curved poloidal filed. A horizontally oblate plasma with the inboard poloidal field null and a natural divertor configuration is formed. The magnetic surfaces are schematically shown in Fig. 1. All poloidal coil currents are kept constant including the current start-up phase. The IPN configuration is formed immediately after ECWs injection and is sustained for a whole discharge duration. The main PWI regions are limited on the divertor rings on the upper and lower part of the centre stack (CS) and on the most inner parts of TB plates, where the scrape off layer (SOL) plasma terminates. The several hot spots and melting parts on the CS cover plates have been observed as a consequence of the severe interaction.

Measurement of the particle fluxes was done with PPs, distributed poloidally from $\theta = -95°$ to 85° (see Fig. 1), where the poloidal angle $\theta = 0$ corresponds to the mid plane, and the origin is at the major radius R = 0.4 m. The LPA, installed at the top plate, was used to analyze the detailed distribution of the Γ_{ion}, estimated from the ion saturation current, at $65° < \theta < 95°$. The locations of the PPs (4,5,6,7), LPA, reciprocating Langmuir probe (RLP) [18], reciprocating permeation probe (RPP; 8) and lines of sight for Hα spectrometry are shown in Fig. 1. The RLP and RPP are located at the same port, and are used to study the radial dependence of the irradiation fluxes along the major radius in the plasma region and beyond the radiation shield to the end of the port.

The positions of PPs in respect to the ECW resonance are shown in Fig. 2. A detailed description of the PPs structure and measuring process is presented in [14]. The diffusion parameters of the PdCu membrane were investigated in [19]. The detection area is 1.2×10^{-3} m^2 for PP4-7 and 7.5×10^{-3} m^2 for PP8, respectively. The radial positions of PP4 and 5 are (0.285–0.345) m and (0.450 – 0.520) m, respectively. In SSTO-2 (Table 1) the radial length of PP4 was the same as of the PP5.

The chamber wall (thick black lines), made of the stainless steel (SS) and tungsten coated SS (blue lines) are the main PFCs. The vessel temperature is always kept at $\sim$ 100 °C. The upper and lower oblique plates ("hot wall" ; tungsten coated SS, gray lines) and vertical plates (radiation shield; SS, vertical gray lines) are in-

Table 1
Parameters of the discharges.

Name	T^{HW}, °C	P_{RF}, kW	f_{RF}, GHz	I_p, kA	$n_e \cdot l$, m^{-2}	R_{res}, m	τ_d, s	shots
SSTO-1	200	30	8.2	8–10	$<10^{17}$	0.286	< 1000	30,169–30,172
SSTO-2	–	50	8.2	16.6	1.2×10^{17}	0.286	< 900	27,394–27,396
ECR-1	200	30	8.2	–	3×10^{17}	0.382	300	30,160–30,165
ECR-2	200	1&11	2.45&8.2	–	$<10^{17}$	0.365 – 1.100	900	32,244–32,250
ECR-3	200	25	8.2	–	$<10^{17}$	0.327	200	30,959–30,967

stalled (except SSTO-2), and their temperature could be kept at $T^{HW} = 200$ °C.

Two kinds of plasma were used - the steady-state tokamak operation (SSTO) with and without hot walls, SSTO-1 and SSTO-2 and an annular slab plasma, ECR-1-3. The operation parameters are summarized in Table 1, where T^{HW} – "hot wall" temperature, P_{RF} – injected RF power, τ_d – discharge duration, I_p – plasma current, f_{RF} – RF frequency. Both SSTO-1 and SSTO-2 were performed with a feedback control of the Hα level aiming at the constant recycling flux. If the H_α level becomes lower than a feedback reference, a gas fuelling is done [20]. The main PWI region in SSTO was on the CS region especially in the range of z = ± (0.6–1) m.

In the ECR plasmas the different resonance positions R_{res} and the different types of the gas fuelling were tested (Fig. 2. and Table 1). ECR-1: a fixed R_{res} (R^1_{res}= 0.38 m) (Fig. 2.), with the second harmonics at $2{\cdot}R^1_{res} = 0.76$ m, the gas was fuelled with piezo valve, 2×10^{20} H injected every 40 sec. ECR-2: a scanning R_{res} from $R^{2-0}_{res} = 0.365$ m to $R^{2-1}_{res} = 1.1$ m with the scanning period of 10 s. 8.2 GHz ECW was injected each 10 s at the maximum toroidal field. The gas fuelling was done with a mass-flow controller with the gas flow rate $q_{gas} = 8.34\times10^{18}$ H/s. ECR-3: fixed R_{res} ($R^3_{res} = 0.33$ m), second harmonics at $2{\cdot}R^3_{res}$= 0.66 m. The gas fuelling was done with the mass-flow controller, $q_{gas} = 5.84\times10^{18}$ H/s. The hydrogen pressure in the ECR plasmas was in range $1–5\times10^{-3}$ Pa and in SSTO plasmas - $1–3\times10^{-4}$ Pa, respectively. Main PWI areas in ECR series were varied on the TB plate with maximum intensity near R_{res} and $2{\cdot}R_{res}$ for each series (Fig. 2.), well separated from the radiation shield at R= 1.3 m, and for ECR-2 it extended close to the 'hot wall'.

3. Experimental results

3.1. Poloidal distribution of the hydrogen incident flux to the walls

Fig. 3 shows a summary of the poloidal distribution of an average value of Φ_i in these five experimental series. Here, $\Phi_i = \int I_i dt$, where I_i is an investigated signal from PPs, LPA or Hα, corresponding to the Γ_{inc}, Γ_{ion} and $I_{H\alpha}$, respectively. For the RPP ($\theta = 0°$) data was used from discharges when probe is inside the port at R = 1.415 m.

In Fig. 3a one can see that Φ_{pp} peaks at $\theta = \pm 90°$ in ECR-2, in which R_{res} was scanned during the discharge and the time averaged PWI area was represented by the location of PP5 ($R^{2-0}_{res} - R^{2-1}_{res}$) and PP4 ($R^3_{res}$). In ECR-1 and 3 the Φ_{PP} values were reduced, though P_{RF} was higher compared to the ECR-2, even though shorter τ_d was taken into account. Φ_{LPA} in ECR-1 has two peaks. The main peak is expected to be close to the central stack, outside the range of the LPA. The detected peak at $\theta \sim 75°$ appears in different slab plasmas as a broad peak which could corresponds to the second harmonic resonance at $2 \cdot R^1_{res}$, outboard plasma diffusion or other phenomena. In the case of 8.2 GHz annular plasma the ion flux to TP plates at the second resonance is several times higher than that at the first resonance. The plasma diffuses in the radial direction mainly towards the lower field. In the slab plasma cases one can expect that the contribution of the atomic flux to the recycling in the inboard side is important, while in the case of the confined plasma it is negligible. Although the ion gradient B drift direction is upwards, an up-down asymmetry was not clearly seen for ECR plasmas, which confirms the conclusion of the dominant neutral contribution. Φ_{LPA} in SSTO-1 and ECR-1 at $\theta > 80°$ are very similar, while Φ_{PP} in the latter is one order magnitude higher than the former. In SSTO-1 $\Phi_{pp}(-90)$ is higher compared to the SSTO-2. In the SSTO-2 PP4 was located further away from CS (see Fig. 2) and the distance of the magnetic field line coming to PP4 from the separatrix was larger, which leads to a smaller contribution of the ions. At the same time the magnetic axis in SSTO-2 was at the larger R, and no 'hat wall' was installed. These two factors should be responsible for higher Φ_{pp} at PP6-8 in SSTO-2 compared to SSTO-1. $\Phi_{pp}(\theta)$ has a local peak at $\theta \sim 0°$ (at RPP). Significant difference of the RPP from other PPs is that it has no cover slit and solid angle with which particles could be collected is much larger than PP6 and 7. As a global aspect of $\Phi_{pp}(\theta)$, the smallest variations in Φ_{pp} at $\theta \sim 0°$ among the discharge types could be coincidental, but also possibly due to less directional sensitivity of the RPP. For more detailed ion flux distributions Φ_{LPA} on the top plate one can see a distinguishable difference between ECR and SSTO plasmas (Fig. 3.b). The main PWI area in ECR-1 is indicated by the enhancement in Φ_{LPA} at $\theta \sim 75°$, which corresponds to the plasma region produced at the second harmonic cyclotron resonance. The reduction tendency in Φ_{LPA} towards the outer walls (smaller θ) seems to be due to the interference of the 'hot wall' and the actual distribution may decay gradually close to the radiation shield. This point will be discussed in Section 3.2. In SSTO-1, since the main PWI area is considered to be on the CS, the distribution tends to decay to the zero level at $\theta < 75°$ as expected. Hα spectroscopy signal varies up to 3 times in case of ECR-1 and SSTO-1,2. In case of the ECR-1 it varies in range of one order of magnitude. The peaks are in the vicinity of the bottom plate ($\theta \sim -75°$), where W limiters are located.

3.2. Radial distribution of the ion and atomic flux in the annular plasma

Radial scan of RPP and RLP in the same discharges (ECR-3) was done to understand differences in atomic and ion fluxes far from the main PWI region both in the plasma side and inside the closed port section with the toroidal dimensions of ~0.5 m. Two regions are separated by the radiation shield at R= 1.3 m. In Fig. 4 time averaged radial profiles of $\langle\Gamma_{inc}\rangle$ and $\langle\Gamma_{ion}\rangle$ are shown with a fluctuating part denoted by vertical bars. Gas fueling was constant in this series and fluctuations in both signals correspond to fluctuations in plasma-wall interaction, not to the pressure change due to gas puff. For R< 1.3 m both $\langle\Gamma_{inc}\rangle$ and $\langle\Gamma_{ion}\rangle$ are smoothly increasing towards the slab plasma. The radial scale lengths and the relative radial profiles of $\langle\Gamma_{inc}\rangle$ and $\langle\Gamma_{ion}\rangle$ are consistent with each other, while a factor of 4–5 difference is seen. It should be noted that these radial profiles inside the plasma side reflect the radially diffusing plasma profile well. There are steep gradients in both $\langle\Gamma_{inc}(R)\rangle$ and $\langle\Gamma_{ion}(R)\rangle$ near R= 1.3 m, indicating that the diffusing plasma terminated by the radiation shield around the torus. For R > 1.3 m $\langle\Gamma_{inc}\rangle$ remains at a finite large value of $\sim 2\times10^{18}$ H/s/m^2, which is ~ 10% of $\langle\Gamma_{inc}\rangle$ at R= 1.1 m (see green dashed line in Fig.

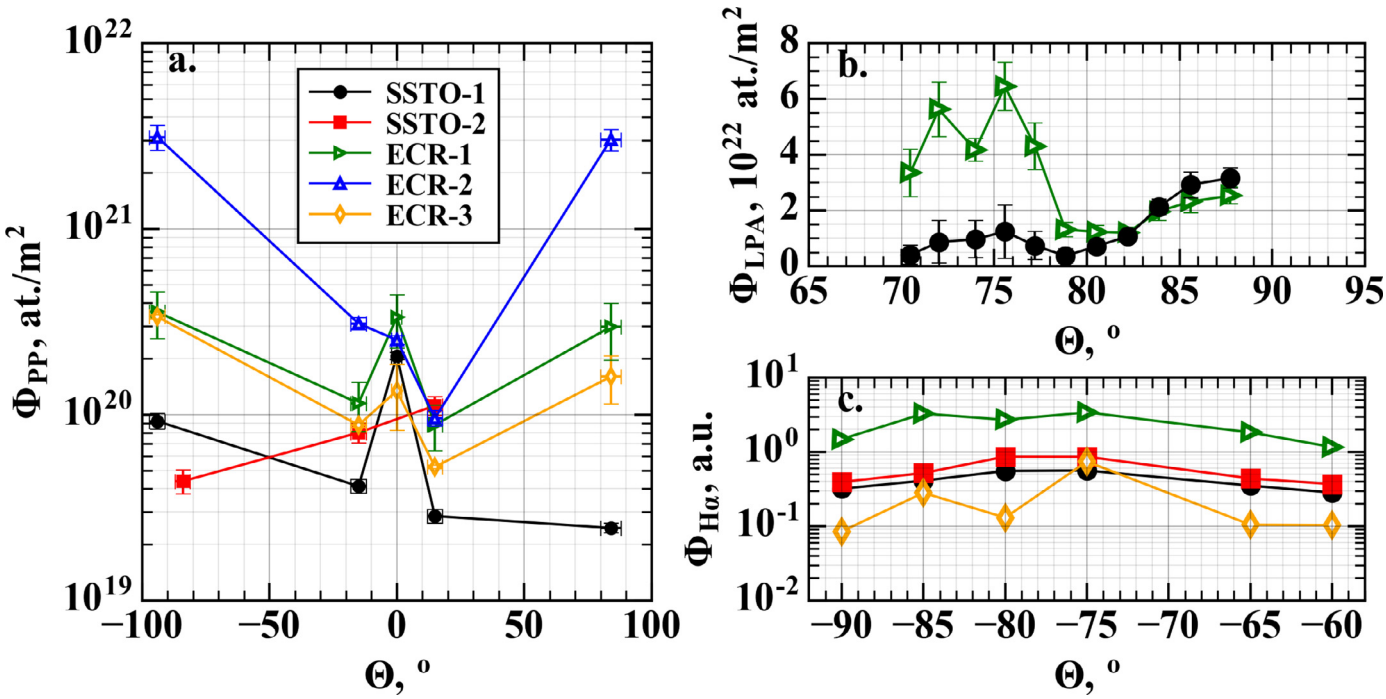

Fig. 3. Poloidal distribution of the particle average irradiation fluence in different sets of discharges, see text. a. Permeation probes, b. Langmuir probes, c. Hα. For RPP ($\theta = 0°$) data was used from discharges when probe is inside the port at R = 1.415 m.

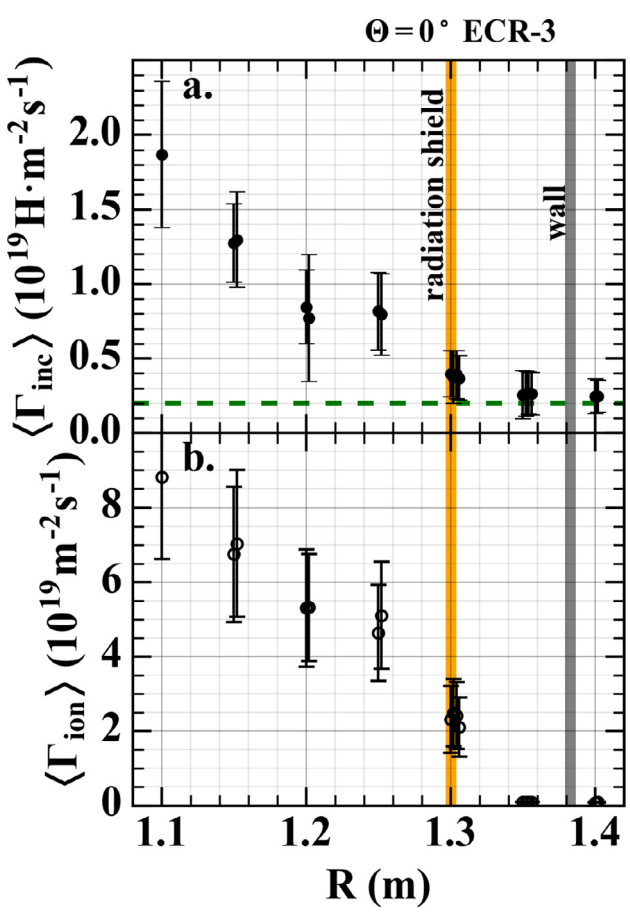

Fig. 4. Radial scan of the irradiation flux by reciprocate probes RPP (a) and RLP (b). Time average values of the fluxes are shown.

4.a), while $\langle\Gamma_{ion}\rangle$ immediately becomes zero. Since there is no gas-driven permeation through the membrane at measured pressures ($P_{max} < 10^{-2}$ Pa) inside the closed section, RPP is registering only atomic flux. The pressure measured in the similar closed port section gives that the molecular hydrogen flux to the PFCs is in the range 3 to 9×10^{19} H/m^2/s if the gas temperature is the same as the wall temperature. By comparison with RPP behind the PFCs, the atomic flux to the walls is smaller by a factor of 15–45. Thus, it can be concluded that the ion flux is dominant inside the PFCs but the atomic hydrogen plays an essential role on the irradiation flux behind the radiation shield or inside the closed port section.

3.3. Hydrogen retention and the effect of the water formation

The hydrogen wall retention was examined by the global gas balance (GGB) method. In Fig. 5 the hydrogen retention ratio R_{GGB} and water concentration C_{H2O} for first three consecutive discharges are plotted for each series. Here $R_{GGB} = N_{wall}/N_{fuel}$, where N_{fuel} is total amount of fueled hydrogen, N_{wall} – number of the retained hydrogen in the wall, determined as to $N_{fuel} - N_{pump}$, where $N_{pump} = N_{H2O} + N_{H2}$; $C_{H2O} = N_{H2O}/(N_{H2O} + N_{H2})$, where N_{H2} - pumped out hydrogen atoms in the form of H_2, N_{H2O} - pumped out water molecules. N_{H2O} is evaluated by taking into account the calibration coefficient for hydrogen gas modified by relative ionization factor [21] and relative molecule mass. As shown in [11], the oxide layer on metals strongly affects the balance between release and retention of hydrogen. Amount of surface oxygen in hydrogen discharges is proportional to water partial pressure and oxygen light emission [22,23]. In present work both water pressure and OII light emission were considered as such indirect indicators of the surface metal oxides.

It was observed that in SSTO-1 the hydrogen release ($N_{wall} < 0$) from the wall was almost one order of magnitude higher than N_{fuel}. In this case the gas was fueled only before plasma production and external fueling was completely replaced by the hydrogen release from the wall, previously retained in ECR-1. Hydrogen release was not significantly reduced during three discharges, and 10

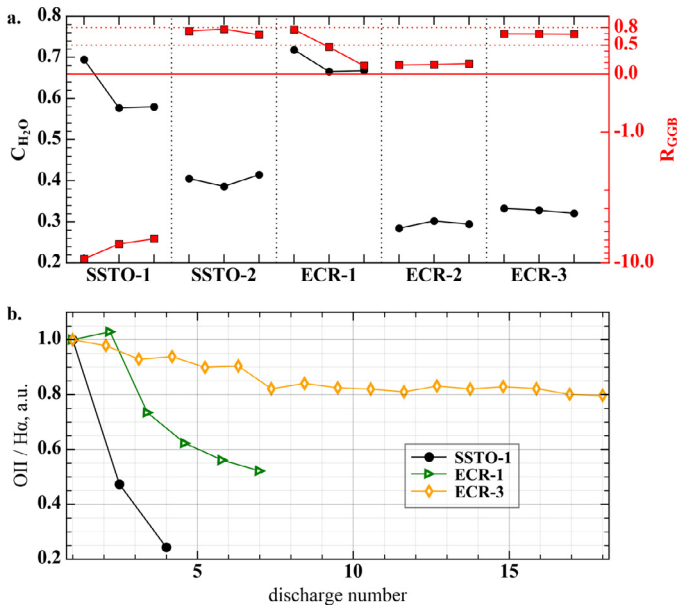

Fig. 5. a. Correlation between water fraction in the pumping flux and the wall retention fraction. b. OII intensity divided by Hα intensity normalized by the first value in the series.

kA plasma current was sustained without H_2 fueling by ECW at 30 kW alone for 1000 sec. In SSTO-2, 16 kA current could be sustained for 820 s with H_2 fueling until 650 sec. In this case, wall retention ($N_{wall} > 0$) was comparable to N_{fuel}. For ECR 1–3 the absolute amount of N_{fuel} is much higher than those in SSTO. Unlike SSTO case, ECR plasma could be sustained steadily in the wide range of N_{fuel} and wall retention fraction.

N_{fuel} was one or two orders smaller than fluxes, irradiating the walls, estimated from Fig. 3 data multiplied by the surface area of PFCs (~ 35 m^2). Thus, it can be considered that fueled particles are highly recycled and final hydrogen retention at the end of the discharge depends on the balance between irradiation and release fluxes.

In SSTO-1 with higher C_{H2O} R_{GGB} is negative. In ECR-1in every shot H_2O is pumped out and C_{H2O} decreases with discharges (Fig. 5a). The OII light emission decreases quickly with the discharge number, indicating the depletion of the surface oxygen. In ECR-1 two processes coexist: reduction of the metal oxides and retention of hydrogen. In SSTO-1 after ECR-1 both partial pressures and the OII emission indicate further decrease of oxygen. In SSTO-1 the plasma density was maintained only by the hydrogen release from the wall. This could be possible due to a) hydrogen stored in the wall in the ECR-1 and b) increased possibility of hydrogen release from metals due to reduced metal oxides, when the barrier for hydrogen recombinative desorption was reduced. In ECR 2 and 3 C_{H2O} was at the steady-state level and in case of ECR-3 OII shows very slow continuous decay in seventeen 300 s ECR plasmas.

4. Discussion

The time evolution of GGB in the long pulse SSTO was studied in a plasma with an inboard limiter configuration (with hot wall) and with low C_{H2O} condition, achieved after several days of tokamak operation. In Fig. 6 temporal changes in the fueling rate, q_{gas}, and wall retention rate, Γ_{wall}, are shown in a 1000 s plasma under the recycling flux constant feedback controlled scenario. In the beginning phase (~100 s) of the discharge q_{gas} increased until the H_α level exceeded a certain feedback level (in this example, ~ 0.3) and R_{GGB} was ~ 1. From 100 s to 200 s feedback worked well and

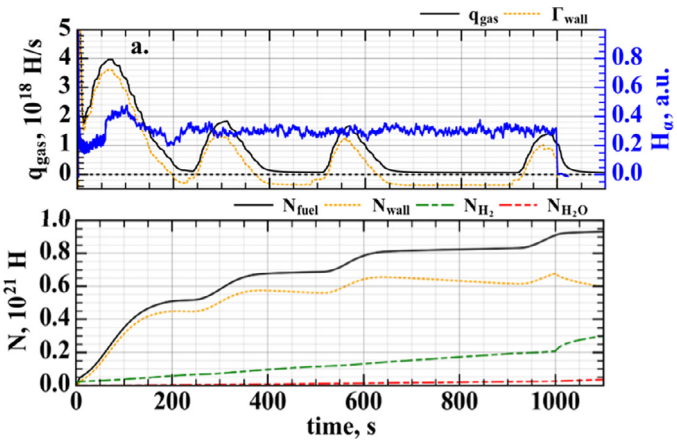

Fig. 6. Time evolution of the apparent wall hydrogen recycling, calculated from global gas balance in the feed-back controlled SSTO (#32,551). a. Gas fueling and wall retention flux with Hα. b. time evolution of the number of fueled, pumped and retained hydrogen.

q_{gas} was gradually reduced. During this phase Γ_{wall} reduced faster than q_{gas} and at ~ 190 s it became negative, indicating the wall release. Within ~ 20 sec the H_α level dropped sharply, after then the feedback started to keep the Hα level constant. During 40 s Γ_{wall} remained at a small constant value so that the total contribution to GGB was small. These processes were repeated twice (from 480 to 520 s and from 880 s to 920 s). At the end of discharge R_{GGB} was down to 0.75. After discharge termination, the hydrogen release was usually enhanced, which corresponds to the net wall release rate without wall retention. This enhancement is commonly seen in all SSTO discharges.

5. Summary

Spatial distribution of the hydrogen wall irradiation fluxes has been directly measured for the first time in different types of long duration discharges with permeation and Langmuir probes, as well as with hydrogen spectroscopy. The poloidal distribution of Γ_{inc} determined by the permeation probes shows that for ECR plasma Γ_{inc} peaks near the main PWI regions, corresponding to the intersecting region of the ECR plasma on the TB plates, and the profile is almost up-down symmetric. For SSTO Γ_{inc} to the TB plate is reduced compared with those near the outer horizontal wall at $\theta \sim 0°$. Γ_{inc} at $\theta \sim 0°$ does not depend on the plasma configuration strongly. Radial distributions of Γ_{inc} and Γ_{ion} are measured along the major radius inside the plasma side and behind the radiation shield on the mid-plane. In the former region, their relative profiles are consistent with each other, suggesting that the main irradiation flux to the PFCs originates from the radially diffusing plasma ions. On the contrary, beyond the PFC Γ_{ion} inside the closed port section can be completely neglected. There it is concluded that Γ_{inc} is dominated by the atomic hydrogen flux. The Γ_{inc} profile behind the PFC is almost constant at $\sim 2 \times 10^{18}$ H/s/m^2, and this net Γ_{inc} to the hydrogen retention is 2–7% of the slow hydrogen molecule flux evaluated by the pressure. Global aspect of the wall retention is also examined by taking into account the water contribution.

Acknowledgments

This work is supported by Grant-in-aid for Scientific Research (S24226020). This work was also performed with the support and under the auspices of the NIFS Collaboration Research Program (NIFS14KOAR017). This work was partially supported in part by the Collaborative Research Program of Research Institute for Applied Mechanics, Kyushu University (26FP-18).

References

[1] O. Ogorodnikova, et al., J. Appl. Phys. 103 (2008) 034902.
[2] L. Begrambekov, et al., Nucl. Instr. Methods Phys. Res. B 315 (2013) 110–116.
[3] W. Shmayda, et al., J. Nucl. Mater. 145-147 (1987) 201.
[4] W. Shmayda, N. Kherani, J. Winter, F. Waelbroeck, J. Nucl. Mater. (1989) 162–164.
[5] S.K. Sharma, et al., FED 85 (2010) 950–955.
[6] H. Zhou, et al., J. Nucl. Mater. 463 (2015) 1066–1077.
[7] A. Kuzmin, et al., J. Nucl. Mater. 463 (2015) 1087–1090.
[8] V. Rohde, V. Mertens, A. Scarabosio, ASDEX Upgrade Team, J. Nucl. Mater. 390–391 (2009) 474–477.
[9] S. Brezinsek, T. Loarer, V. Philipps, et al., Nucl. Fusion 53 (2013) 083023.
[10] K. Hanada, et al., J. Nucl. Mater. 463 (2015) 1084–1086.
[11] L. Begrambekov, et al., J. Surf. Inv. X-Ray Synch. Neutr. Tech. 9-1 (2015) 190–195.
[12] S.K. Sharma, H. Zushi, N. Yoshida, et al., Fusion Eng. Design 85 (2012) 77.
[13] K. Hanada, et al., Plasma Sci. Technol. 13 (2011) 307–311.
[14] A. Kuzmin, et al., Vacuum 129 (2016) 178–182.
[15] S.K. Sharma, H. Zushi, I. Takagi, et al., J. Nucl. Mater. 420 (2012) 83.
[16] S. Tashima, H. Zushi, et al., NF 54 (2014) 023010.
[17] K. Mishra, H. Zushi, et al., NF 55 (2015) 083009.
[18] T. Onchi, H. Zushi, et al., Plasma Phys. Control. Fusion 58 (2016) 115004.
[19] M. Onaka, I. Takagi, et al., Nucl. Mater. Energy 9 (2016) 104–108.
[20] M. Hasegawa, et al., FED 96-97 (2015) 629–632.
[21] F. Nakao, Vacuum 25 (9-10) (1975) 431–435.
[22] L. Oren, R.J. Taylor, Nucl. Fusion 176 (1977) 1143–1151.
[23] Y. Sakamoto, et al., 93&94 (1980) 333–337.